Coordinate Interleaved OFDM With Repeated In-Phase/Quadrature Index Modulation

Omer Furkan Tugtekin, *Student Member, IEEE*, Ali Tugberk Dogukan, *Student Member, IEEE*, Emre Arslan, *Student Member, IEEE*, and Ertugrul Basar, *Fellow, IEEE*

***Abstract*— Orthogonal frequency division multiplexing with index modulation (OFDM-IM), which transmits information bits through ordinary constellation symbols and indices of active subcarriers, is a promising multicarrier transmission scheme and has attracted the attention of researchers due to numerous benefits such as flexibility and simplicity. Nonetheless, OFDM-IM cannot satisfy the needs of future wireless communication services such as superior reliability, high data rates, and low complexity. In this article, we propose a novel OFDM-IM scheme named coordinate interleaved OFDM with repeated in-phase/quadrature IM (CI-OFDM-RIQIM), which provides superior error performance and enhanced spectral efficiency due to its diversity order of two and clever subcarrier activation pattern (SAP) detection mechanism, respectively. In addition, CI-OFDM-RIQIM is further extended to coordinate interleaved OFDM with in-phase/quadrature IM (CI-OFDM-IQIM) by doubling information bits transmitted by IM. Furthermore, log-likelihood ratio (LLR) based low-complexity detectors are designed for both proposed schemes. Theoretical analyses are performed and an upper bound on the bit error probability is derived. Comprehensive computer simulations under perfect and imperfect channel state information (CSI), are conducted to compare the proposed and reference schemes. It is shown that CI-OFDM-RIQIM and CI-OFDM-IQIM show superior results and can be considered promising candidates for next-generation wireless communication systems.**

***Index Terms*— OFDM, index modulation, coordinate interleaving, diversity gain.**

I. Introduction

ORTHOGONAL frequency division multiplexing (OFDM) with index modulation (IM) [1] which transmits additional information bits through the indices of the active subcarriers, is a promising OFDM-based multicarrier transmission scheme. Since information bits are more preserved against fading when they are transmitted by IM rather than classical M-ary PSK/QAM modulation, OFDM-IM shows superior error performance over the conventional OFDM. Moreover, OFDM-IM attracts much attention in the literature due to its several advantages such as high flexibility and implementation simplicity. To further enhance the flexibility, OFDM with generalized IM (OFDM-GIM), in which the number of active subcarriers in a subblock is no longer fixed, is proposed in [2]. In addition, the spectral efficiency of OFDM-IM has been improved by OFDM with in-phase/quadrature IM (OFDM-IQ-IM) [3], [4] where IM is performed on in-phase and quadrature components independently, doubling the number of IM bits. Moreover, OFDM with subcarrier number modulation (OFDM-SNM) is proposed in [5], where the number of the active subcarriers in a subblock is determined by incoming data bits, resulting in enhanced spectral efficiency. By choosing subcarrier activation patterns (SAPs) across multiple layers, a layered OFDM-IM approach has been developed to increase the number of bits conveyed by IM [6]. Additionally, a block interleaver is employed in the subcarrier level in [7] to improve the error performance of OFDM-IM. In [8], rectangular differential coding is applied to OFDM-IM, where channel state information (CSI) is no longer required at the receiver side to detect information bits. Furthermore, many schemes have been proposed to address the diverse requirements of 5G services such as improved reliability, higher spectral and energy efficiency, and low complexity, by utilizing the flexibility of IM. For example, OFDM with hybrid number and IM (OFDM-HNIM) [9] and sparse-encoded codebook IM (SE-CBIM) [10] are introduced to meet the requirements of different 5G services such as massive machine type communications (mMTC) and ultra-reliable low-latency communications (URLLC), respectively. Due to its simple and flexible structure, OFDM-IM can be combined with several emerging wireless communication systems such as multiple-input multiple-output (MIMO) [11], [12], [13], [14], non-orthogonal multiple access (NOMA) [15], [16], [17], [18], [19], joint radar communication [20], and optical communication systems [21], [22].

Due to its de-activated subcarriers, it is challenging for OFDM-IM to provide high spectral efficiency. With this purpose, dual-mode aided OFDM (DM-OFDM) is proposed in [23], where null subcarriers are modulated by a secondary distinguishable constellation to transmit data symbols. The authors in [24], extend the work in [23] to a generalized form by varying the number of subcarriers modulated by the same mode. To further increase the number of bits transmitted

Manuscript received 4 August 2022; revised 25 December 2022 and 20 March 2023; accepted 9 May 2023. Date of publication 23 May 2023; date of current version 9 January 2024. This work was supported in part by the Scientific and Technological Research Council of Turkey (TUBITAK) 2244 Project under Grant 119C157 and in part by Vestel Electronics. The associate editor coordinating the review of this article and approving it for publication was X. Tao. *(Corresponding author: Ertugrul Basar.)*

The authors are with the Communications Research and Innovation Laboratory (CoreLab), Department of Electrical and Electronics Engineering, Koç University, Sariyer, 34450 Istanbul, Turkey (e-mail: otugtekin15@ku.edu.tr; adogukan18@ku.edu.tr; earslan18@ku.edu.tr; ebasar@ku.edu.tr).

Color versions of one or more figures in this article are available at https://doi.org/10.1109/TWC.2023.3276178.

Digital Object Identifier 10.1109/TWC.2023.3276178

by IM, multiple-mode OFDM-IM (MM-OFDM-IM), which exploits multiple signal constellations and their full permutations to perform IM, is proposed in [25]. MM-OFDM-IM is generalized in [26], where the size of the constellations can be different from each other while the number of bits transmitted via IM remains unchanged. $\mathcal{Q}$-ary MM-OFDM-IM ($\mathcal{Q}$-MM-OFDM-IM) is proposed in [27], where each subcarrier is modulated by $\mathcal{Q}$ disjoint M-ary constellations repeatedly and a maximum-distance separable (MDS) code is utilized in the indices of these constellations, resulting in a higher number of index symbols. Furthermore, OFDM implementations with MDS amplitude and phase modulation (MDS-APM) and MDS in-phase and quadrature modulation (MDS-IQM) are given in [28]. Super-mode OFDM-IM (SuM-OFDM-IM) [29], which jointly determines mode activation patterns (MAPs) and SAPs is proposed to further increase the number of information bits transmitted by IM. OFDM with set partition modulation (OFDM-SPM), which differentiates subsets in a set partition by distinguishable constellations to achieve better error performance, is proposed in [30]. In addition, OFDM with transmit diversity (OFDM-TD), where null subcarriers are activated to convey the same information with active subcarriers by utilizing multiple constellations, is proposed in [31]. Since all subcarriers are activated, these schemes can achieve higher spectral efficiency values than OFDM-IM. Therefore, they can be considered as candidate schemes for future enhanced mobile broadband (eMBB) services such as augmented/virtual reality (AR/VR).

To combat multi-path fading in wireless communication systems and provide better reliability, numerous OFDM-IM-based schemes, which yield additional diversity gain, are proposed in the literature. Repeated IM-OFDM (ReMO), which transmits the same data symbol over the activated subcarriers to achieve a transmit diversity, is proposed in [32]. Moreover, coded OFDM-IM is incorporated with a simple transmit diversity scheme to enhance the error performance of OFDM-IM [33]. Coordinate interleaved OFDM-IM (CI-OFDM-IM) [34] transmits the real and imaginary parts of the data symbols over different subcarriers and provides a diversity order of two. Another novel scheme called OFDM with power distribution IM (OFDM-PIM) that provides additional diversity gain by conveying data symbols through two subcarriers with high and low power levels, is introduced in [35]. As a promising scheme, CI-OFDM-PIM that ensures a diversity gain that is equal to the subblock size, is presented in [36]. In this scheme, coordinate interleaved data symbols are distributed over two distinct subcarriers with high and low power levels. In [37], repeated IM-OFDM with CI (RIM-OFDM-CI) is proposed, where data symbols from different clusters are coordinate interleaved. Furthermore, the same indices of subcarriers in both clusters are exploited to transmit the coordinate interleaved data symbols resulting in improved detection of index bits. It has been demonstrated that RIM-OFDM-CI provides a better error performance than OFDM-IM and CI-OFDM-IM at the same spectral efficiency. In [38], the authors extend their work in [37] by optimizing the rotation angle for the signal constellation with detailed theoretical analysis and developing low-complexity detectors to reduce receiver complexity. Furthermore, a comprehensive survey about OFDM-IM-based schemes is presented in [39]. Despite these remarkable improvements in the literature, there is still an obvious necessity for OFDM-IM-based waveform designs that can provide superior error performance without sacrificing spectral efficiency. In this perspective, we have focused on increasing the number of additional data bits transmitted by IM while still providing a solid diversity gain.

In this paper, we propose a novel OFDM-IM-based transmission scheme named *coordinate interleaved OFDM with repeated in-phase/quadrature IM (CI-OFDM-RIQIM)*, which provides additional diversity gain compared to conventional OFDM-IM. In contrast to CI-OFDM-IM, all subblocks are first divided into two clusters with equal sizes, in the proposed scheme. Then, different from RIM-OFDM-CI, more than 1 SAPs are cleverly determined thanks to performing IM to in-phase/quadrature components separately. The real and imaginary parts from the first half of the data symbol vector are transmitted over the active subcarriers in the first and second clusters, respectively. Moreover, the real and imaginary parts of the second half of the data symbol vector are transmitted over the active subcarriers in the second and first clusters, respectively. Since the same SAPs are exploited to transmit the real and imaginary parts of data symbols, information bits conveyed by IM are more preserved. Furthermore, we extend our work to another scheme called *coordinate interleaved OFDM with in-phase/quadrature IM (CI-OFDM-IQIM)*, where information bits transmitted by IM are doubled thanks to applying in-phase/quadrature indexing four times. Different from the first proposed scheme, four distinct SAPs are determined by the incoming data bits to transmit the real and imaginary parts of the first and second halves of data symbol vector. Since the real and imaginary parts of each data symbol are conveyed over two distinct subcarriers, a diversity order of two is guaranteed in both schemes. In addition, low-complexity detectors for proposed schemes are designed where index bits and data symbols are decoded by log-likelihood ratio (LLR) based method and single symbol detection, respectively. An upper bound for the average bit error probability (ABEP) is derived. Furthermore, a diversity analysis is performed, and an optimum rotation angle selection strategy is presented. Finally, error performance comparisons between the proposed and benchmark schemes are presented through comprehensive computer simulations under perfect and imperfect CSI.

The remainder of this article is organized as follows. In Section II, the system models for the proposed schemes and their LLR detectors are introduced. In Section III, performance analyses such as theoretical BER upper bound, diversity analysis and optimization, are given. Section IV presents computer simulation results to compare the proposed scheme and its benchmarks in terms of error performance. Finally, Section V concludes the paper.

Notations: Bold, lowercase, and capital letters stand for vectors and matrices, respectively. $(\cdot)^{\mathrm{H}}$ and $(\cdot)^{\mathrm{T}}$ are used for Hermitian and transposition operations, respectively. $\mathbf{I}_{N\times N}$ refer to $N \times N$ identify matrix. The determinant and rank

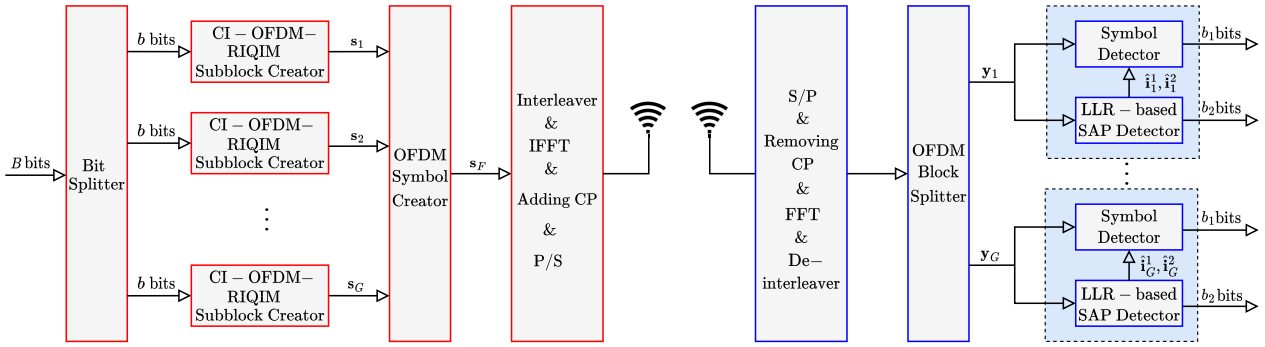

Fig. 1. Transceiver architecture of CI-OFDM-RIQIM.

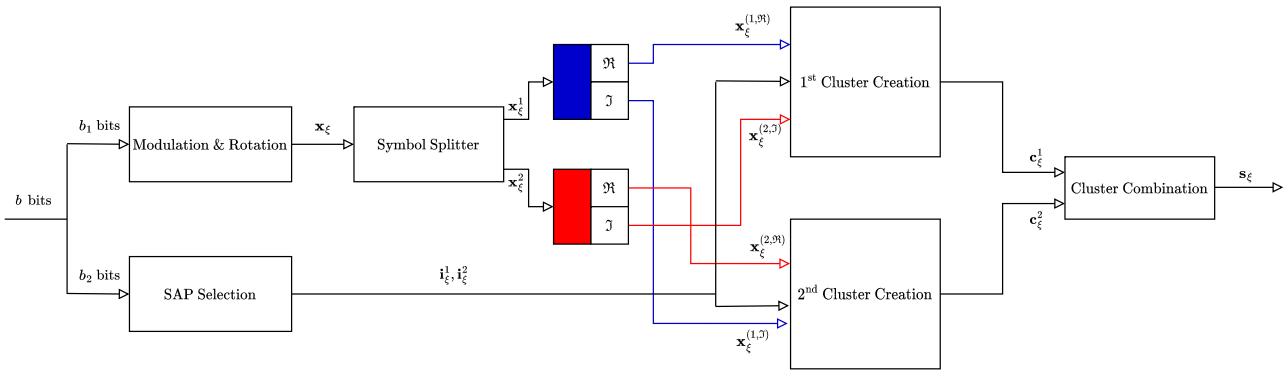

Fig. 2. CI-OFDM-RIQIM Subblock Creator.

of a matrix is represented by $\det(\cdot)$ and $\mathrm{rank}(\cdot)$, respectively. $X \sim \mathcal{CN}(0, \sigma_X^2)$ denotes the distribution of a circularly symmetric complex Gaussian random variable X with variance σ_X^2. Binomial coefficient is represented by $\binom{n}{k}$. $\|\cdot\|$, $E\{\cdot\}$, and $\lfloor\cdot\rfloor$ are used for Euclidean norm, expectation, and floor function, respectively.

II. System Model

In this section, we first introduce the system model of CI-OFDM-RIQIM. Furthermore, the system model of the second proposed scheme, called CI-OFDM-IQIM, is presented.

A. CI-OFDM-RIQIM

CI-OFDM-RIQIM is an OFDM-based transmission system including a total number of N_F subcarriers. As seen from Fig. 1, a total number of B bits enter the system and these bits are then split into G groups of b bits, $b = B/G$. Each group of b bits is exploited to create a CI-OFDM-RIQIM subblock with size $N_S = N_F/G$, where N_S is an even number and greater than 2. Moreover, each subblock is divided into two clusters of length $N_C = N_S/2$. It is sufficient to investigate the formation of the ξ^{th} subblock $\mathbf{s}_\xi$, since the same processes are performed to constitute each subblock, where $\xi = 1, \cdots, G$. To create $\mathbf{s}_\xi$, b bits are separated into two groups with b_1 and b_2 bits. Firstly, $b_1 = 2K \log_2 M$ bits determine the ξ^{th} data symbol vector $\mathbf{x}_\xi = [x_{\xi,1}, \cdots, x_{\xi,2K}]^{\text{T}}$, $x_{\xi,\kappa} \in \mathcal{M}^\theta$, $\kappa = 1, \cdots, 2K$, where K and $\mathcal{M}^\theta$ are the number of active subcarriers in a cluster and M-ary constellation rotated by an angle θ, respectively. Note that constellation rotation is necessary to harvest diversity in CI-based schemes [40]. Then, $\mathbf{x}_\xi$ is split into two parts: $\mathbf{x}_\xi^1 = [x_{\xi,1}, \cdots, x_{\xi,K}]$ and $\mathbf{x}_\xi^2 = [x_{\xi,K+1}, \cdots, x_{\xi,2K}]$, $\mathbf{x}_\xi = [(\mathbf{x}_\xi^1)^{\text{T}}, (\mathbf{x}_\xi^2)^{\text{T}}]^{\text{T}}$ and the real and imaginary parts of these vectors are obtained as $\mathbf{x}_\xi^1 = \mathbf{x}_\xi^{(1,\Re)} + j\mathbf{x}_\xi^{(1,\Im)}$ and $\mathbf{x}_\xi^2 = \mathbf{x}_\xi^{(2,\Re)} + j\mathbf{x}_\xi^{(2,\Im)}$. Secondly, by using combinatorial method or a look-up table [1], the λ^{th} subcarrier activation pattern (SAP), $\mathbf{i}_\xi^\lambda = [i_{\xi,1}^\lambda, \cdots, i_{\xi,K}^\lambda]^{\text{T}}$, $i_{\xi,k}^\lambda \in \{1, \cdots, N\}$, $k = 1, \cdots, K$, is selected by $b_2/2 = \lfloor \log_2 \binom{N_C}{K} \rfloor$ bits, where $\lambda = 1, 2$. Here, a total number of $b_2 = 2\lfloor \log_2 \binom{N_C}{K} \rfloor$ bits are transmitted via the selected SAPs $(\mathbf{i}_\xi^1, \mathbf{i}_\xi^2)$. Subsequently, the entries of $\mathbf{x}^{(1,R)}$ and $\mathbf{x}^{(2,\Im)}$ are inserted into the first cluster $\mathbf{c}_\xi^1 = [c_{\xi,1}^1, \cdots, c_{\xi,N_C}^1]$ with the entries of $\mathbf{i}_\xi^1$ and $\mathbf{i}_\xi^2$, respectively. Moreover, the entries of $\mathbf{x}^{(2,\Re)}$ and $\mathbf{x}^{(1,I)}$ are inserted into the second cluster $\mathbf{c}_\xi^2 = [c_{\xi,1}^2, \cdots, c_{\xi,N_C}^2]$ with the entries of $\mathbf{i}_\xi^2$ and $\mathbf{i}_\xi^1$, respectively. Then, the ξ^{th} subblock is obtained as $\mathbf{s}_\xi = [(\mathbf{c}_\xi^1)^{\text{T}}, (\mathbf{c}_\xi^2)^{\text{T}}]^{\text{T}} = [s_{\xi,1}, \cdots, s_{\xi,N_S}]^{\text{T}}$, where $s_{\xi,\mu} \in \{0, \mathcal{M}^{(\theta,\Re)}, j\mathcal{M}^{(\theta,\Im)}, \tilde{\mathcal{M}}\}$, $\mu = 1, \cdots, N_S$, $\mathcal{M}^{(\theta,\Re)}$ and $\mathcal{M}^{(\theta,\Im)}$ are the real and imaginary parts of the rotated constellation $\mathcal{M}^\theta$, respectively. Additionally, $\tilde{\mathcal{M}}$ is a M^2-ary constellation whose each element is in the form of $x_1^\Re + jx_2^\Im$, where $x_1^\Re \in \mathcal{M}^{(\theta,\Re)}$ and $x_2^\Im \in \mathcal{M}^{(\theta,\Im)}$. Hence, the number of bits transmitted by the ξ^{th} CI-OFDM-RIQIM subblock is expressed as:

$$b = 2K \log_2 M + 2 \left\lfloor \log_2 \binom{N_C}{K} \right\rfloor. \tag{1}$$

Finally, by concatenating all subblocks, the overall transmitted OFDM symbol is obtained as $\mathbf{s}_F = [\mathbf{s}_1^{\text{T}}, \cdots, \mathbf{s}_G^{\text{T}}]^{\text{T}}$. Note that in this scheme, CI is not directly applied to the

TABLE I
ALL CI-OFDM-RIQIM SUBBLOCK REALIZATIONS FOR $N_C = 4$ AND $K = 2$

First $b_2/2$ bits	Second $b_2/2$ bits	$(\mathbf{i}^1)^{\mathrm{T}}$	$(\mathbf{i}^2)^{\mathrm{T}}$	Subblock $(\mathbf{s}^{\mathrm{T}})$							
				s_1	s_2	s_3	s_4	s_5	s_6	s_7	s_8
{0 0}	{0 0}	[1 3]	[1 3]	$x_1^{\Re}+jx_3^{\Im}$	0	$x_2^{\Re}+jx_4^{\Im}$	0	$x_3^{\Re}+jx_1^{\Im}$	0	$x_4^{\Re}+jx_2^{\Im}$	0
{0 0}	{0 1}	[1 3]	[2 4]	$x_1^{\Re}$	$jx_3^{\Im}$	$x_2^{\Re}$	$jx_4^{\Im}$	$jx_1^{\Im}$	$x_3^{\Re}$	$jx_2^{\Im}$	$x_4^{\Re}$
{0 0}	{1 0}	[1 3]	[1 4]	$x_1^{\Re}+jx_3^{\Im}$	0	$x_2^{\Re}$	$jx_4^{\Im}$	$x_3^{\Re}+jx_1^{\Im}$	0	$jx_2^{\Im}$	$x_4^{\Re}$
{0 0}	{1 1}	[1 3]	[2 3]	$x_1^{\Re}$	$jx_3^{\Im}$	$x_2^{\Re}+jx_4^{\Im}$	0	$jx_1^{\Im}$	$x_3^{\Re}$	$x_4^{\Re}+jx_2^{\Im}$	0
{0 1}	{0 0}	[2 4]	[1 3]	$jx_3^{\Im}$	$x_1^{\Re}$	$jx_4^{\Im}$	$x_2^{\Re}$	$x_3^{\Re}$	$jx_1^{\Im}$	$x_4^{\Re}$	$jx_2^{\Im}$
{0 1}	{0 1}	[2 4]	[2 4]	0	$x_1^{\Re}+jx_3^{\Im}$	0	$x_2^{\Re}+jx_4^{\Im}$	0	$x_3^{\Re}+jx_1^{\Im}$	0	$x_4^{\Re}+jx_2^{\Im}$
{0 1}	{1 0}	[2 4]	[1 4]	$jx_3^{\Im}$	$x_1^{\Re}$	0	$x_2^{\Re}+jx_4^{\Im}$	$x_3^{\Re}$	$jx_1^{\Im}$	0	$x_4^{\Re}+jx_2^{\Im}$
{0 1}	{1 1}	[2 4]	[2 3]	0	$x_1^{\Re}+jx_3^{\Im}$	$jx_4^{\Im}$	$x_2^{\Re}$	0	$x_3^{\Re}+jx_1^{\Im}$	$x_4^{\Re}$	$jx_2^{\Im}$
{1 0}	{0 0}	[1 4]	[1 3]	$x_1^{\Re}+jx_3^{\Im}$	0	$jx_4^{\Im}$	$x_2^{\Re}$	$x_3^{\Re}+jx_1^{\Im}$	0	$x_4^{\Re}$	$jx_2^{\Im}$
{1 0}	{0 1}	[1 4]	[2 4]	$x_1^{\Re}$	$jx_3^{\Im}$	0	$x_2^{\Re}+jx_4^{\Im}$	$jx_1^{\Im}$	$x_3^{\Re}$	0	$x_4^{\Re}+jx_2^{\Im}$
{1 0}	{1 0}	[1 4]	[1 4]	$x_1^{\Re}+jx_3^{\Im}$	0	0	$x_2^{\Re}+jx_4^{\Im}$	$x_3^{\Re}+jx_1^{\Im}$	0	0	$x_4^{\Re}+jx_2^{\Im}$
{1 0}	{1 1}	[1 4]	[2 3]	$x_1^{\Re}$	$jx_3^{\Im}$	$jx_4^{\Im}$	$x_2^{\Re}$	$jx_1^{\Im}$	$x_3^{\Re}$	$x_4^{\Re}$	$jx_2^{\Im}$
{1 1}	{0 0}	[2 3]	[1 3]	$jx_3^{\Im}$	$x_1^{\Re}$	$x_2^{\Re}+jx_4^{\Im}$	0	$x_3^{\Re}$	$jx_1^{\Im}$	$x_4^{\Re}+jx_2^{\Im}$	0
{1 1}	{0 1}	[2 3]	[2 4]	0	$x_1^{\Re}+jx_3^{\Im}$	$x_2^{\Re}$	$jx_4^{\Re}$	0	$x_3^{\Re}+jx_1^{\Im}$	$jx_2^{\Im}$	$x_4^{\Re}$
{1 1}	{1 0}	[2 3]	[1 4]	$jx_3^{\Im}$	$x_1^{\Re}$	$x_2^{\Re}$	$jx_4^{\Im}$	$x_3^{\Re}$	$jx_1^{\Im}$	$jx_2^{\Im}$	$x_4^{\Re}$
{1 1}	{1 1}	[2 3]	[2 3]	0	$x_1^{\Re}+jx_3^{\Im}$	$x_2^{\Re}+jx_4^{\Im}$	0	0	$x_3^{\Re}+jx_1^{\Im}$	0	$x_4^{\Re}+jx_2^{\Im}$

data symbols as in [34]; however, after placing the data symbols into the subblock, a number of data symbols might be coordinate interleaved.

For better illustration, we provide a mapping example for the creation of all subblocks with specified parameters. Since the same processes are applied for each subblock, we remove the subscript ξ here. Assuming $N_C = 4$, $K = 2$, $N_S = 8$, all possible subblocks are presented in Table I.

After forming the overall OFDM symbol by repeating the same procedure for all subblocks, a block-type interleaver is employed as in [34]. The time domain signal is acquired by taking an inverse fast Fourier Transform (IFFT). After adding a cyclic prefix (CP) with length L to the beginning of the OFDM frame and employing parallel to serial (P/S) and digital/analog transformation, the time-domain OFDM signal is transmitted through a T-tap frequency-selective Rayleigh fading channel with channel impulse response (CIR) coefficients

$$\mathbf{h}_T = [h_T(1) \cdots h_T(T)]^{\mathrm{T}}, \tag{2}$$

where $h_T(\beta), \beta = 1, \cdots, T$ follows circularly symmetric complex Gaussian random variables with the $\mathcal{CN}(0, 1/T)$.

At the receiver part, to obtain the signal in the frequency domain, first, the CP is removed, and then FFT and deinterleaving are exploited. Finally, the equivalent input-output relationship corresponding to ξ in the frequency domain can be given by

$$\mathbf{y}_\xi = \mathbf{S}_\xi \mathbf{h}_\xi + \mathbf{n}_\xi, \tag{3}$$

where $\mathbf{S}_\xi = \mathrm{diag}(\mathbf{s}_\xi)$, $\mathbf{y}_\xi$, $\mathbf{h}_\xi$, and $\mathbf{n}_\xi$ represent the transmitted signal, received signal vector, channel coefficients, and noise samples vector corresponding to the ξ^{th} subblock, respectively. The distributions of the elements of $\mathbf{n}_\xi$ and $\mathbf{h}_\xi$ are $\mathcal{CN}(0, N_0)$ and $\mathcal{CN}(0, 1)$, respectively, where N_0 is the noise variance. By ignoring the effect of CP, the spectral efficiency is obtained as $\eta = B/N_F$.

The maximum-likelihood (ML) detection can be performed to detect the ξ^{th} subblock by utilizing the set $\mathcal{S} = \{\mathbf{s}(1), \mathbf{s}(2), \cdots, \mathbf{s}(2^b)\}$ which contains all possible subblock realizations:

$$\hat{\mathbf{s}}_\xi = \arg\min_{\mathbf{s}_\xi \in \mathcal{S}} \|\mathbf{y}_\xi - \mathbf{S}_\xi \mathbf{h}_\xi\|^2. \tag{4}$$

Since the ML detector searches for all possible of SAPs and data symbols in an exhaustive manner, it becomes unfeasible to exploit this detector for higher values of N_S, K, and M. Thus, we also present an LLR-based detector for CI-OFDM-RIQIM to reduce the detection complexity.

B. Low-Complexity LLR Detector for CI-OFDM-RIQIM

The proposed LLR detector aims to detect the CI-OFDM-RIQIM symbol subblock-by-subblock. For simplicity, we remove the subscript ξ.

The inputs of Algorithm 1 are given as follows:

- New received signal vector that is equalized by zero-forcing (ZF) equalizer: $\bar{\mathbf{y}} = [\bar{y}_1, \cdots, \bar{y}_{N_S}]^{\mathrm{T}}$, $\bar{y}_\mu = y_\mu / h_\mu$, $\mu = 1, \cdots, N_S$.
- Four different constellation sets: $\mathcal{M}_1 = \{\mathcal{M}^{(\theta,\Re)}, \mathcal{M}^\star\}$, $\mathcal{M}_2 = \{\mathcal{M}^{(\theta,\Im)}, \mathcal{M}'\}$, $\mathcal{M}_3 = \{\mathcal{M}^{(\theta,\Im)}, \mathcal{M}'\}$, and $\mathcal{M}_4 = \{\mathcal{M}^{(\theta,\Re)}, \mathcal{M}'\}$, where $\mathcal{M}^\star$ and $\mathcal{M}'$ are the M^2-ary constellations whose elements are in the form of $x_1^{\Re} + jx_2^{\Im}$ and $x_2^{\Re} + jx_1^{\Im}$, respectively, $(x_1, x_2) \in \mathcal{M}^\theta$.
- A set including all legal SAPs: $\mathcal{I} = \{\mathbf{i}_1, \cdots, \mathbf{i}_{2^{b_2/2}}\}$
- Noise variance: N_0.

The major steps of Algorithm 1 are discussed as follows:

1) The log-likelihood (LL) value of the c^{th} subcarrier being a symbol from the constellation set $\mathcal{M}_1$ and being null, is calculated at lines 3 and 4, respectively.
2) The LL value of the $(c + N_C)^{\mathrm{th}}$ subcarrier being a symbol from the constellation set $\mathcal{M}_2$ and being null, is calculated at lines 5 and 6, respectively.
3) The LL value of the c^{th} subcarrier being a symbol from the constellation set $\mathcal{M}_3$ and being null, is calculated at lines 7 and 8, respectively.
4) The LL value of the $(c + N_C)^{\mathrm{th}}$ subcarrier being a symbol from the constellation set $\mathcal{M}_4$ and being null, is calculated at lines 9 and 10, respectively.

Algorithm 1 Low-Complexity LLR-Based SAP Detector for CI-OFDM-RIQIM

Input: $\bar{\mathbf{y}}$, N_0, $\mathcal{M}_1$, $\mathcal{M}_2$, $\mathcal{M}_3$, $\mathcal{M}_4$, $\mathcal{I}$
Output: $\hat{\mathbf{i}}^1$, $\hat{\mathbf{i}}^2$

1: **for** $c = 1$ **to** N_C **do**
2: **for** $\chi = 1$ **to** $M^2 + M$ **do**
3: $\Delta^{\Re}_{(1,1)} = -\frac{|h(c)|^2}{N_0}|\bar{y}^{\Re}(c) - \mathcal{M}_1(\chi)|^2$
4: $\Delta^{\Re}_{(1,2)} = -\frac{|h(c)|^2}{N_0}|\bar{y}^{\Re}(c)|^2$
5: $\Delta^{\Im}_{(2,1)} = -\frac{|h(N_C+c)|^2}{N_0}|\bar{y}^{\Im}(N_C + c) - \mathcal{M}_2(\chi)|^2$
6: $\Delta^{\Im}_{(2,2)} = -\frac{|h(N_C+c)|^2}{N_0}|\bar{y}^{\Im}(N_C + c)|^2$
7: $\Delta^{\Im}_{(1,1)} = -\frac{|h(c)|^2}{N_0}|\bar{y}^{\Im}(c) - \mathcal{M}_3(\chi)|^2$
8: $\Delta^{\Im}_{(1,2)} = -\frac{|h(c)|^2}{N_0}|\bar{y}^{\Im}(c)|^2$
9: $\Delta^{\Re}_{(2,1)} = -\frac{|h(N_C+c)|^2}{N_0}|\bar{y}^{\Re}(N_C + c) - \mathcal{M}_4(\chi)|^2$
10: $\Delta^{\Re}_{(2,2)} = -\frac{|h(N_C+c)|^2}{N_0}|\bar{y}^{\Re}(N_C + c)|^2$
11: $\mathbf{\Lambda}_1(\chi, c) = \Delta^{\Re}_{(1,1)} - \Delta^{\Re}_{(1,2)} + \Delta^{\Im}_{(2,1)} - \Delta^{\Im}_{(2,2)}$
12: $\mathbf{\Lambda}_1(\chi, c) = \mathbf{\Lambda}_1(\chi, c) + \log(K) - \log(N_C - K)$
13: $\mathbf{\Lambda}_2(\chi, c) = \Delta^{\Im}_{(1,1)} - \Delta^{\Im}_{(1,2)} + \Delta^{\Re}_{(2,1)} - \Delta^{\Re}_{(2,2)}$
14: $\mathbf{\Lambda}_2(\chi, c) = \mathbf{\Lambda}_2(\chi, c) + \log(K) - \log(N_C - K)$
15: **end for**
16: $\Xi_1 = \mathbf{\Lambda}_1(1, c)$
17: $\Xi_2 = \mathbf{\Lambda}_2(1, c)$
18: **for** $\chi = 2$ **to** $M^2 + M$ **do**
19: $\psi_1 = \log(1 + \exp(-|\Xi_1 - \mathbf{\Lambda}_1(\chi, c)|))$
20: $\psi_2 = \log(1 + \exp(-|\Xi_2 - \mathbf{\Lambda}_2(\chi, c)|))$
21: $T_1 = \max(\Xi_1, \mathbf{\Lambda}_1(\chi, c)) + \psi_1$
22: $T_2 = \max(\Xi_2, \mathbf{\Lambda}_2(\chi, c)) + \psi_2$
23: $\Xi_1 = T_1$
24: $\Xi_2 = T_2$
25: **end for**
26: $\Omega_1(c) = \Xi_1$
27: $\Omega_2(c) = \Xi_2$
28: **end for**
29: **for** $\beta = 1$ **to** $2^{b_2/2}$ **do**
30: $\Omega'_1(\beta) = \sum_k \Omega_1(\mathcal{I}_\beta(k))$
31: $\Omega'_2(\beta) = \sum_k \Omega_2(\mathcal{I}_\beta(k))$
32: **end for**
33: $\hat{\mathbf{i}}^1 = \mathcal{I}_{\max(\Omega'_1)}$
34: $\hat{\mathbf{i}}^2 = \mathcal{I}_{\max(\Omega'_2)}$

5) The calculated LL values are combined between lines (11-14). Note that $\mathbf{\Lambda}_\lambda(\chi, c)$ is the element located in the χ^{th} row and c^{th} column of the matrix $\mathbf{\Lambda}_\lambda$, $\lambda = 1, 2$.
6) The joint LLR value corresponding to the c^{th} subcarrier of cluster 1 and 2 is calculated between lines (16-27).
7) The LLR values are combined according to the legal SAPs between lines (29-32). Note that $\mathcal{I}_\beta(k)$ represents the k^{th} element of the β^{th} SAP.
8) The detected SAPs $(\hat{\mathbf{i}}^1, \hat{\mathbf{i}}^2)$ are provided between lines (33-34). Note that the function $\max(\breve{\Omega}_\lambda)$ gives the index of the maximum value of $\breve{\Omega}_\lambda$.

After obtaining $(\hat{\mathbf{i}}^1, \hat{\mathbf{i}}^2)$, the equivalent model as in [34] is exploited to detect the k^{th} data symbol corresponding to the λ^{th} half of the data symbol vector $\mathbf{x}^\lambda$ as follows:

$$\hat{x}^\lambda_k = \min_{x \in \mathcal{M}^\theta} \|\breve{\mathbf{y}}^\lambda_k - \breve{\mathbf{H}}^\lambda_k [x^{\Re}\ x^{\Im}]^{\mathrm{T}}\|^2, \tag{6}$$

where $\breve{\mathbf{y}}^\lambda_k$ and $\breve{\mathbf{H}}^\lambda_k$ are given in (5), as shown at the bottom of the page, $\lambda = 1, 2$.

C. CI-OFDM-IQIM

CI-OFDM-IQIM can be considered as an extension of CI-OFDM-RIQIM, where information bits conveyed by IM are doubled. As in CI-OFDM-RIQIM, to create the ξ^{th} subblock, a total number of $b_1 = 2K \log_2 M$ bits first determine the data symbol vector $\mathbf{x}_\xi = [x_{\xi,1}, \cdots, x_{\xi,2K}]^{\mathrm{T}}$. Then, the data symbol vectors $\mathbf{x}^{(1,\Re)}_\xi$, $\mathbf{x}^{(2,\Re)}_\xi$, $\mathbf{x}^{(1,\Im)}_\xi$, and $\mathbf{x}^{(2,\Im)}_\xi$ are obtained similarly as in CI-OFDM-RIQIM. Moreover, $b_2 = 4\lfloor \log_2 \binom{N_C}{K} \rfloor$ bits are separated into four groups, each group of $b_2/4$ bits determines an SAP $\mathbf{i}^\nu_\xi = [i^\nu_{\xi,1}, \cdots, i^\nu_{\xi,K}]^{\mathrm{T}}$, $i^\nu_{\xi,k} \in \{1, \cdots, N\}$, $k = 1, \cdots, K$, $\nu = 1, \cdots, 4$. The entries of $\mathbf{x}^{(1,R)}_\xi$ and $\mathbf{x}^{(2,\Im)}_\xi$ are placed into the first cluster $\mathbf{c}^1_\xi$ with the entries of $\mathbf{i}^1_\xi$ and $\mathbf{i}^4_\xi$, respectively. Moreover, the entries of $\mathbf{x}^{(2,\Re)}_\xi$ and $\mathbf{x}^{(1,I)}_\xi$ are placed into the second cluster $\mathbf{c}^2_\xi$ with the entries of $\mathbf{i}^3_\xi$ and $\mathbf{i}^2_\xi$, respectively. Hence, the ξ^{th} subblock is obtained as $\mathbf{s}_\xi = [(\mathbf{c}^1_\xi)^{\mathrm{T}}, (\mathbf{c}^2_\xi)^{\mathrm{T}}]^{\mathrm{T}}$. The number of bits transmitted by a single CI-OFDM-IQIM subblock is given by

$$b = 2K \log_2 M + 4 \left\lfloor \log_2 \binom{N_C}{K} \right\rfloor. \tag{7}$$

As seen from (7), compared to CI-OFDM-RIQIM, the number of index bits is doubled in CI-OFDM-IQIM.

For simplicity, we provide an example that demonstrates the creation of a CI-OFDM-IQIM subblock. We remove the subscript ξ for the ease of presentation.

Example: Assume that $N_C = 4$, $K = 2$, $\mathbf{i}^1 = [1, 3]^T$, $\mathbf{i}^2 = [1, 4]^T$, $\mathbf{i}^3 = [2, 3]^T$, and $\mathbf{i}^4 = [2, 3]^T$. With these parameters, an example subblock is obtained as:

$$\mathbf{s} = [x^{\Re}_1, j\ x^{\Im}_3, x^{\Re}_2 + jx^{\Im}_4, 0 | jx^{\Im}_1, x^{\Re}_3, x^{\Re}_4, j\ x^{\Im}_2]^{\mathrm{T}}. \tag{8}$$

The ML detection rule as in (4) can be exploited to detect both data symbols and SAPs.

$$\breve{\mathbf{y}}^\lambda_k = \begin{bmatrix} \mathbf{y}^{\Re}(\hat{\mathbf{i}}^\lambda(k)) \\ \mathbf{y}^{\Im}(\hat{\mathbf{i}}^\lambda(k)) \\ \mathbf{y}^{\Re}(\hat{\mathbf{i}}^\lambda(k) + N_C) \\ \mathbf{y}^{\Im}(\hat{\mathbf{i}}^\lambda(k) + N_C) \end{bmatrix}, \breve{\mathbf{H}}^1_k = \begin{bmatrix} \mathbf{h}^{\Re}(\hat{\mathbf{i}}^1(k)) & 0 \\ \mathbf{h}^{\Im}(\hat{\mathbf{i}}^1(k)) & 0 \\ 0 & -\mathbf{h}^{\Im}(\hat{\mathbf{i}}^1(k) + N_C) \\ 0 & \mathbf{h}^{\Re}(\hat{\mathbf{i}}^1(k) + N_C) \end{bmatrix}, \breve{\mathbf{H}}^2_k = \begin{bmatrix} 0 & -\mathbf{h}^{\Im}(\hat{\mathbf{i}}^2(k)) \\ 0 & \mathbf{h}^{\Re}(\hat{\mathbf{i}}^2(k)) \\ \mathbf{h}^{\Re}(\hat{\mathbf{i}}^2(k) + N_C) & 0 \\ \mathbf{h}^{\Im}(\hat{\mathbf{i}}^2(k) + N_C) & 0 \end{bmatrix} \tag{5}$$

Algorithm 2 Low-Complexity LLR-Based SAP Detector for CI-OFDM-IQIM

Input: $\bar{\mathbf{y}}$, N_0, $\mathcal{M}^{(\theta,\Re)}$, $\mathcal{M}^{(\theta,\Im)}$, $\mathcal{I}$
Output: $\hat{\mathbf{i}}^1$, $\hat{\mathbf{i}}^2$, $\hat{\mathbf{i}}^3$, $\hat{\mathbf{i}}^4$

1: **for** $c = 1$ **to** N_C **do**
2: **for** $\chi = 1$ **to** M **do**
3: $\Delta^{\Re}_{(1,1)} = -\frac{|h(c)|^2}{N_0}|\bar{y}^{\Re}(c) - \mathcal{M}^{(\theta,\Re)}(\chi)|^2$
4: $\Delta^{\Re}_{(1,2)} = -\frac{|h(c)|^2}{N_0}|\bar{y}^{\Re}(c)|^2$
5: $\Delta^{\Re}_{(2,1)} = -\frac{|h(N_C+c)|^2}{N_0}|\bar{y}^{\Re}(N_C+c) - \mathcal{M}^{(\theta,\Re)}(\chi)|^2$
6: $\Delta^{\Re}_{(2,2)} = -\frac{|h(N_C+c)|^2}{N_0}|\bar{y}^{\Re}(N_C+c)|^2$
7: $\Delta^{\Im}_{(1,1)} = -\frac{|h(c)|^2}{N_0}|\bar{y}^{\Im}(c) - \mathcal{M}^{(\theta,\Im)}(\chi)|^2$
8: $\Delta^{\Im}_{(1,2)} = -\frac{|h(c)|^2}{N_0}|\bar{y}^{\Im}(c)|^2$
9: $\Delta^{\Im}_{(2,1)} = -\frac{|h(N_C+c)|^2}{N_0}|\bar{y}^{\Im}(N_C+c) - \mathcal{M}^{(\theta,\Im)}(\chi)|^2$
10: $\Delta^{\Im}_{(2,2)} = -\frac{|h(N_C+c)|^2}{N_0}|\bar{y}^{\Im}(N_C+c)|^2$
11: $\mathbf{\Lambda}^{\Re}_1(\chi,c) = \Delta^{\Re}_{(1,1)} - \Delta^{\Re}_{(1,2)} + \log(\frac{K}{N_C-K})$
12: $\mathbf{\Lambda}^{\Re}_2(\chi,c) = \Delta^{\Re}_{(2,1)} - \Delta^{\Re}_{(2,2)} + \log(\frac{K}{N_C-K})$
13: $\mathbf{\Lambda}^{\Im}_1(\chi,c) = \Delta^{\Im}_{(1,1)} - \Delta^{\Im}_{(1,2)} + \log(\frac{K}{N_C-K})$
14: $\mathbf{\Lambda}^{\Im}_2(\chi,c) = \Delta^{\Im}_{(2,1)} - \Delta^{\Im}_{(2,2)} + \log(\frac{K}{N_C-K})$
15: **end for**
16: $\Xi^{\Re}_1 = \mathbf{\Lambda}^{\Re}_1(1,c)$
17: $\Xi^{\Re}_2 = \mathbf{\Lambda}^{\Re}_2(1,c)$
18: $\Xi^{\Im}_1 = \mathbf{\Lambda}^{\Im}_1(1,c)$
19: $\Xi^{\Im}_2 = \mathbf{\Lambda}^{\Im}_2(1,c)$
20: **for** $\chi = 2$ **to** M **do**
21: $\psi^{\Re}_1 = \log(1+\exp(-|\Xi^{\Re}_1 - \mathbf{\Lambda}^{\Re}_1(\chi,c)|))$
22: $\psi^{\Re}_2 = \log(1+\exp(-|\Xi^{\Re}_2 - \mathbf{\Lambda}^{\Re}_2(\chi,c)|))$
23: $\psi^{\Im}_1 = \log(1+\exp(-|\Xi^{\Im}_1 - \mathbf{\Lambda}^{\Im}_1(\chi,c)|))$
24: $\psi^{\Im}_2 = \log(1+\exp(-|\Xi^{\Im}_2 - \mathbf{\Lambda}^{\Im}_2(\chi,c)|))$
25: $T^{\Re}_1 = \max(\Xi^{\Re}_1, \mathbf{\Lambda}^{\Re}_1(\chi,c)) + \psi^{\Re}_1$
26: $T^{\Re}_2 = \max(\Xi^{\Re}_2, \mathbf{\Lambda}^{\Re}_2(\chi,c)) + \psi^{\Re}_2$
27: $T^{\Im}_1 = \max(\Xi^{\Im}_1, \mathbf{\Lambda}^{\Im}_1(\chi,c)) + \psi^{\Im}_1$
28: $T^{\Im}_2 = \max(\Xi^{\Im}_2, \mathbf{\Lambda}^{\Im}_2(\chi,c)) + \psi^{\Im}_2$
29: $\Xi^{\Re}_1 = T^{\Re}_1$
30: $\Xi^{\Re}_2 = T^{\Re}_2$
31: $\Xi^{\Im}_1 = T^{\Im}_1$
32: $\Xi^{\Im}_2 = T^{\Im}_2$
33: **end for**
34: $\Omega^{\Re}_1(c) = \Xi^{\Re}_1$
35: $\Omega^{\Re}_2(c) = \Xi^{\Re}_2$
36: $\Omega^{\Im}_1(c) = \Xi^{\Im}_1$
37: $\Omega^{\Im}_2(c) = \Xi^{\Im}_2$
38: **end for**
39: **for** $\beta = 1$ **to** $2^{b_2/2}$ **do**
40: $\breve{\Omega}^{\Re}_1(\beta) = \sum_k \Omega^{\Re}_1(\mathcal{I}_\beta(k))$
41: $\breve{\Omega}^{\Re}_2(\beta) = \sum_k \Omega^{\Re}_2(\mathcal{I}_\beta(k))$
42: $\breve{\Omega}^{\Im}_1(\beta) = \sum_k \Omega^{\Im}_1(\mathcal{I}_\beta(k))$
43: $\breve{\Omega}^{\Im}_2(\beta) = \sum_k \Omega^{\Im}_2(\mathcal{I}_\beta(k))$
44: **end for**
45: $\hat{\mathbf{i}}^1 = \mathcal{I}_{\max(\breve{\Omega}^{\Re}_1)}$
46: $\hat{\mathbf{i}}^2 = \mathcal{I}_{\max(\breve{\Omega}^{\Im}_1)}$
47: $\hat{\mathbf{i}}^3 = \mathcal{I}_{\max(\breve{\Omega}^{\Re}_2)}$
48: $\hat{\mathbf{i}}^4 = \mathcal{I}_{\max(\breve{\Omega}^{\Im}_2)}$

D. Low-Complexity LLR Detector for CI-OFDM-IQIM

The proposed LLR detector aims to detect the CI-OFDM-IQIM symbol subblock-by-subblock. For simplicity, we remove the subscript ξ again.

The inputs of Algorithm 2 are given as follows:

- New received signal vector with zero-forcing (ZF) equalizer: $\bar{\mathbf{y}} = [\bar{y}_1, \cdots, \bar{y}_{N_S}]^{\mathrm{T}}$, $\bar{y}_\mu = y_\mu/h_\mu$, $\mu = 1, \cdots, N_S$.
- Two different constellation sets: $\mathcal{M}^{(\theta,\Re)}$, $\mathcal{M}^{(\theta,\Im)}$.
- A set including all legal SAPs: $\mathcal{I} = \{\mathbf{i}_1, \cdots, \mathbf{i}_{2^{b_2/2}}\}$
- Noise variance: N_0.

The major steps of Algorithm 2 are discussed below:

1) The LLR value of the c^{th} subcarrier is calculated between lines (1-38).
2) The LLR values are combined according to the legal SAPs between lines (39-44). Note that $\mathcal{I}_\beta(k)$ represents the k^{th} element of the β^{th} SAP.
3) The detected SAPs $(\hat{\mathbf{i}}^1, \hat{\mathbf{i}}^2, \hat{\mathbf{i}}^3, \hat{\mathbf{i}}^4)$ are provided between lines (45-48). Note that the function $\max(\breve{\Omega}_\lambda)$ gives the index of the maximum value of $\breve{\Omega}_\lambda$.

After obtaining $(\hat{\mathbf{i}}^1, \hat{\mathbf{i}}^2, \hat{\mathbf{i}}^3, \hat{\mathbf{i}}^4)$, the equivalent model is utilized to detect the k^{th} data symbol corresponding to the λ^{th} half of the data symbol vector $\mathbf{x}^\lambda$ as follows:

$$\hat{x}^\lambda_k = \min_{x \in \mathcal{M}^\theta} \|\breve{\mathbf{y}}^\lambda_k - \breve{\mathbf{H}}^\lambda_k [x^{\Re}\ x^{\Im}]^{\mathrm{T}}\|^2, \tag{9}$$

where $\breve{\mathbf{y}}^\lambda_k$ and $\breve{\mathbf{H}}^\lambda_k$ are given in (10), as shown at the bottom of the next page, for $\lambda = 1, 2$.

III. Performance Analysis

In this section, we derive the theoretical upper bound of the bit error probability (BEP) for the proposed schemes. In addition, we analyze the diversity order of the proposed schemes. Furthermore, an optimization strategy on the θ value is given to minimize the BER, resulting in superior error performance.

A. Theoretical Upper Bound on BEP

In this subsection, an upper bound for the BEP of the proposed schemes is derived by employing ML detection. By utilizing (4), the conditional pairwise error probability (CPEP) which can be defined as the probability of erroneously detecting $\hat{\mathbf{S}}$ while transmitting $\mathbf{S}$ conditioned on $\mathbf{h}$, is expressed as:

$$\mathrm{P}(\mathbf{S} \to \hat{\mathbf{S}}|\mathbf{h}) = \mathrm{Q}\left(\sqrt{\frac{E_b}{2N_0}\left|\left|(\mathbf{S}-\hat{\mathbf{S}})\mathbf{h}\right|\right|^2}\right), \tag{11}$$

where E_b is the average transmitted energy per bit and defined as $E_b = (N_F + T)/B$. Then, by taking the approximation of $\mathrm{Q}(x) \approx \frac{e^{-2x^2/3}}{4} + \frac{e^{-x^2/2}}{12}$ into consideration, the unconditioned PEP (UPEP) can be derived as in [1]:

$$\begin{aligned}\mathrm{P}(\mathbf{S} \to \hat{\mathbf{S}}) &= E_{\mathbf{h}}\{\mathrm{P}(\mathbf{S} \to \hat{\mathbf{S}}|\mathbf{h})\} \\ &\approx \frac{1/4}{\det(\mathbf{I}_{N_S} + \phi_1 \mathbf{A})} + \frac{1/12}{\det(\mathbf{I}_{N_S} + \phi_2 \mathbf{A})},\end{aligned} \tag{12}$$

where $\phi_1 = 1/3N_0$, $\phi_2 = 1/4N_0$, and $\mathbf{A} = (\mathbf{S} - \hat{\mathbf{S}})^{\mathrm{H}}(\mathbf{S} - \hat{\mathbf{S}})$ is the $N_s \times N_s$ difference matrix. Then, the BER of the CI-OFDM-RIQIM can be upper bounded by:

$$P_b \leq \frac{1}{b2^b} \sum_{\mathbf{S}} \sum_{\hat{\mathbf{S}}} \mathrm{P}(\mathbf{S} \to \hat{\mathbf{S}}) \mathrm{e}(\mathbf{S}, \hat{\mathbf{S}}), \tag{13}$$

where $\mathrm{e}(\mathbf{S}, \hat{\mathbf{S}})$ is the number of faulty bits when $\mathbf{S}$ is transmitted, but erroneously detected as $\hat{\mathbf{S}}$.

B. Diversity Analysis

In this subsection, we investigate the diversity order of CI-OFDM-RIQIM and CI-OFDM-IQIM by considering two cases: (a) erroneous detection of index bits while data symbols are correctly decoded and (b) erroneous detection of single or multiple data symbols while index bits are correctly decoded. For case (a), assume that subblock $\mathbf{s}$ with the parameters $(\mathrm{i}^1)^{\mathrm{T}} = [1, 3]$ and $(\mathrm{i}^2)^{\mathrm{T}} = [1, 3]$ is transmitted; however, subblock $\hat{\mathbf{s}}$ with the parameters $(\hat{\mathrm{i}}^1)^{\mathrm{T}} = [1, 3]$ and $(\hat{\mathrm{i}}^2)^{\mathrm{T}} = [1, 4]$ is erroneously decoded for the given parameters $N_C = 4$ and $K = 2$ while data symbols are correctly decoded. This error event can be expressed as:

$$\begin{aligned} \mathbf{s} \to \hat{\mathbf{s}} = &[x_1^{\Re} + jx_3^{\Im}, 0, x_2^{\Re} + jx_4^{\Im}, 0 | x_3^{\Re} + jx_1^{\Im}, 0, x_4^{\Re} + jx_2^{\Im}, 0] \\ &\to [x_1^{\Re} + jx_3^{\Im}, 0, x_2^{\Re}, j\ x_4^{\Im} | x_3^{\Re} + jx_1^{\Im}, 0, jx_2^{\Im}, x_4^{\Re}]. \end{aligned} \tag{14}$$

This specific example is the worst-case event and provides a diversity order of $\Gamma = 2$, where $\Gamma = \mathrm{rank}(\mathbf{A})$. For case ($b$), assume that subblock $\mathbf{s}$ with data symbols (x_1, x_2, x_3, x_4), is transmitted; however, subblock $\hat{\mathbf{s}}$ with a single symbol error $(\hat{x_1}, x_2, x_3, x_4)$, is erroneously decoded while indices $(\mathrm{i}^1)^{\mathrm{T}} = [1, 3]$ and $(\mathrm{i}^2)^{\mathrm{T}} = [1, 3]$ are correctly detected, $N_C = 4$, and $K = 2$. This error event can be stated as follows:

$$\begin{aligned} \mathbf{s} \to \hat{\mathbf{s}} = &[x_1^{\Re} + jx_3^{\Im}, 0, x_2^{\Re} + jx_4^{\Im}, 0 | x_3^{\Re} + jx_1^{\Im}, 0, x_4^{\Re} + jx_2^{\Im}, 0] \\ &\to [\hat{x}_1^{\Re} + jx_3^{\Im}, 0, x_2^{\Re} + jx_4^{\Im}, 0 | x_3^{\Re} + j\hat{x}_1^{\Im}, 0, x_4^{\Re} + jx_2^{\Im}, 0]. \end{aligned} \tag{15}$$

As seen from (15), even erroneous detection of a single data symbol causes changes over two separated subcarriers and; thus, a diversity order of $\Gamma = 2$ is guaranteed. Eventually, the proposed schemes ensure $\min_{\mathbf{S}, \hat{\mathbf{S}}}(\Gamma) = 2$, which proves that the diversity order of CI-OFDM-RIQIM and CI-OFDM-IQIM is 2.

Moreover, total numbers of error events that have a rank value of $\Gamma = 2$, 3, 4, 5, 6, 7 and 8, are presented in Fig. 3 to give further insight into the performance of the proposed scheme for $N_S = 8$ at spectral efficiency of 1.25 bps/Hz. As it can be concluded from Fig. 3, CI-OFDM-RIQIM provides more error events with $\Gamma = 8$ compared to RIM-OFDM-CI and CI-OFDM-IM, resulting in superior error performance.

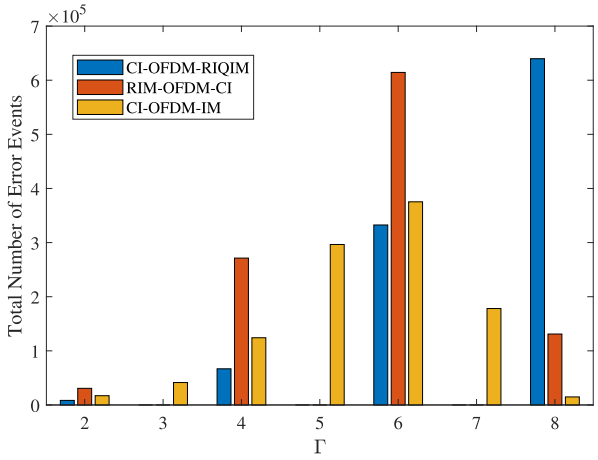

Fig. 3. Total number of error events with $\Gamma = 2, \cdots, 8$ for CI-OFDM-RIQM and benchmark schemes.

C. Optimization

In this subsection, we find the optimum θ value which minimizes the BER by searching θ values from 1° to 89°. with increments of 1°. Note that since the quadrature amplitude modulation (QAM) constellation repeats itself every 90°, we do not examine beyond this angle. The angle that provides the lowest BER at a selected SNR value, is selected as the optimum angle for the system. For example, as seen in Fig. 4(a), with the given parameters $N_C = 4$ and $K = 2$, the optimum θ for CI-OFDM-RIQIM system is obtained as 63° and 22° for 4-QAM and 8-QAM, respectively, when SNR is fixed to 15 dB. Moreover, we use the proposed LLR detectors to find an optimum rotation angle for higher modulation orders since it is not feasible to determine the optimum angle by employing ML detection. For instance, θ is obtained as 72° and 18° for 16-QAM and 64-QAM, respectively as seen from Fig. 4(b).

IV. Simulation Results and Comparisons

In this section, CI-OFDM-RIQIM and CI-OFDM-IQIM are compared with various OFDM-IM-based reference schemes via computer simulations, given that all simulations are

$$\breve{\mathbf{y}}_k^1 = \begin{bmatrix} \mathbf{y}^{\Re}(\hat{\mathbf{i}}^1(k)) \\ \mathbf{y}^{\Im}(\hat{\mathbf{i}}^1(k)) \\ \mathbf{y}^{\Re}(\hat{\mathbf{i}}^2(k) + N_C) \\ \mathbf{y}^{\Im}(\hat{\mathbf{i}}^2(k) + N_C) \end{bmatrix}, \breve{\mathbf{y}}_k^2 = \begin{bmatrix} \mathbf{y}^{\Re}(\hat{\mathbf{i}}^4(k)) \\ \mathbf{y}^{\Im}(\hat{\mathbf{i}}^4(k)) \\ \mathbf{y}^{\Re}(\hat{\mathbf{i}}^3(k) + N_C) \\ \mathbf{y}^{\Im}(\hat{\mathbf{i}}^3(k) + N_C) \end{bmatrix}$$

$$\breve{\mathbf{H}}_k^1 = \begin{bmatrix} \mathbf{h}^{\Re}(\hat{\mathbf{i}}^1(k)) & 0 \\ \mathbf{h}^{\Im}(\hat{\mathbf{i}}^1(k)) & 0 \\ 0 & -\mathbf{h}^{\Im}(\hat{\mathbf{i}}^2(k) + N_C) \\ 0 & \mathbf{h}^{\Re}(\hat{\mathbf{i}}^2(k) + N_C) \end{bmatrix}, \breve{\mathbf{H}}_k^2 = \begin{bmatrix} 0 & -\mathbf{h}^{\Im}(\hat{\mathbf{i}}^4(k)) \\ 0 & \mathbf{h}^{\Re}(\hat{\mathbf{i}}^4(k)) \\ \mathbf{h}^{\Re}(\hat{\mathbf{i}}^3(k) + N_C) & 0 \\ \mathbf{h}^{\Im}(\hat{\mathbf{i}}^3(k) + N_C) & 0 \end{bmatrix} \tag{10}$$

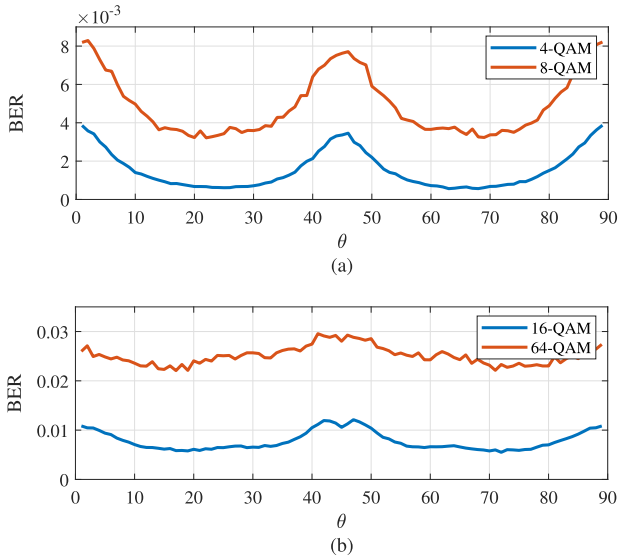

Fig. 4. Optimum rotation angle search for (a) 4-QAM and 8-QAM using ML detector (b) 16-QAM and 64-QAM using LLR detector, when $N_C = 4$, $K = 2$, and SNR is fixed to 15 dB.

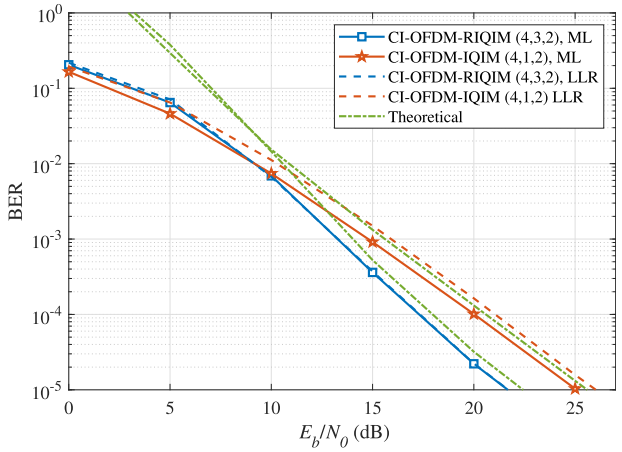

Fig. 5. Error performance of CI-OFDM-RIQIM and CI-OFDM-IQIM for the cases where ML and LLR detectors are utilized at a spectral efficiency of 1.25 bps/Hz.

realized with the system parameters of $N_F = 128$, $L = 16$, and $T = 10$ tap Rayleigh fading channel. For the sake of simplicity, we will define "OFDM-IM (N_S,K,M)", "OFDM-IQ-IM (N_S,K,M)", "CI-OFDM-IM (N_S,K,M)", and "ReMO (N_S,K,M)" as OFDM-IM, OFDM-IQ-IM, CI-OFDM-IM, and ReMO schemes, respectively, where K out of N_S subcarriers are activated in one subblock and M is the modulation order. Moreover, we will refer to "RIM-OFDM-CI (N_C,K,M)", "CI-OFDM-RIQIM (N_C,K,M)", and "CI-OFDM-IQIM" (N_C,K,M)" as RIM-OFDM-CI, CI-OFDM-RIQIM, and CI-OFDM-IQIM schemes, respectively, where K subcarriers are active in one cluster with size N_C while M is the modulation order. Note that optimum rotation angles for simulations of the proposed schemes have been determined based on the optimization strategy explained in Section III.

As shown in Fig. 5, theoretical BER curves that are acquired by (13), are an accurate upper bound for CI-OFDM-RIQIM and CI-OFDM-IQIM. In addition, as seen in Fig. 5, the proposed LLR detector for CI-OFDM-RIQIM has considerable

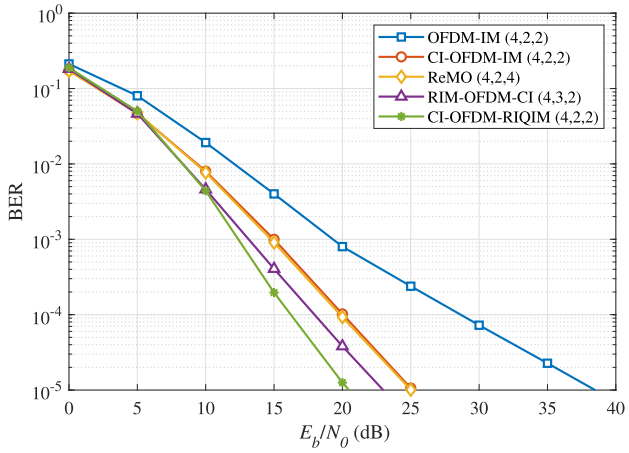

Fig. 6. Error performance comparison of CI-OFDM-RIQIM with benchmark schemes at a spectral efficiency of 1 bps/Hz.

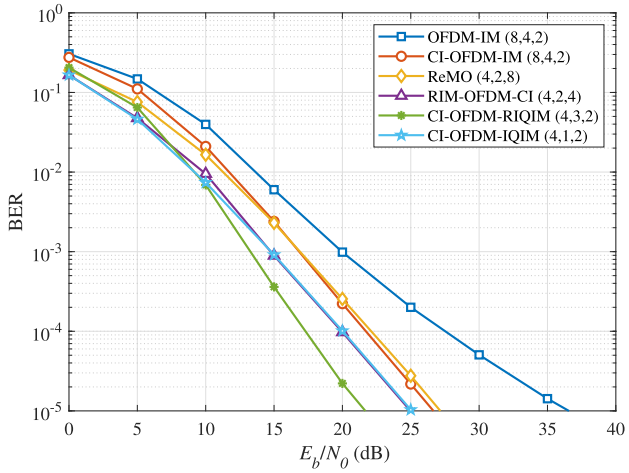

Fig. 7. Error performance comparison of CI-OFDM-RIQIM and CI-OFDM-IQIM with benchmark schemes at a spectral efficiency of 1.25 bps/Hz.

close error performance compared to the BER performance obtained by ML detector while having reduced complexity. On the other hand, since the indices of the active subcarriers are not repeated in CI-OFDM-IQIM, the proposed LLR detector provides a slightly worse error performance than the ML detector.

As seen from Fig. 6, CI-OFDM-RIQIM provides superior error performance compared to the benchmark schemes at spectral efficiency of 1 bps/Hz. CI-OFDM-RIQIM has approximately 3 dB, 5 dB, and 17 dB SNR gain over RIM-OFDM-CI, CI-OFDM-IM, and OFDM-IM, respectively, although less number of subcarriers are activated in one cluster due to the increased number of transmitted IM bits.

In Fig. 7, the error performance of CI-OFDM-RIQIM, CI-OFDM-IQIM, and reference schemes is investigated at spectral efficiency of 1.25 bps/Hz. It is observed that CI-OFDM-RIQIM outperforms all benchmark schemes in terms of error performance. More specifically, CI-OFDM-RIQIM provides almost a 4 dB gain over the nearest benchmark while utilizing a lower modulation order due to the doubled number of IM bits. Moreover, approximately the same error performance of RIM-OFDM-CI is obtained

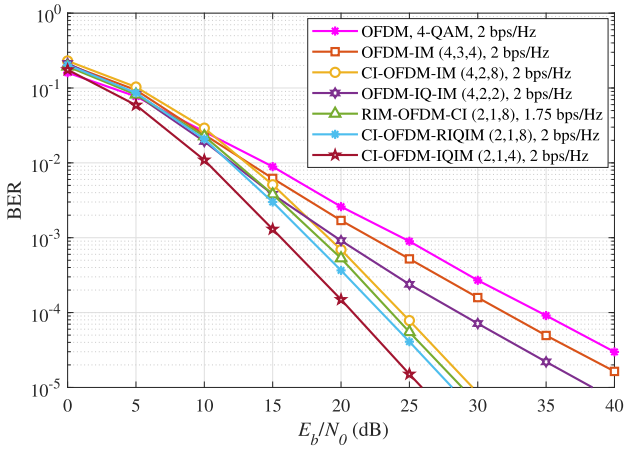

Fig. 8. Error performance comparison of CI-OFDM-RIQIM and CI-OFDM-IQIM with benchmark schemes.

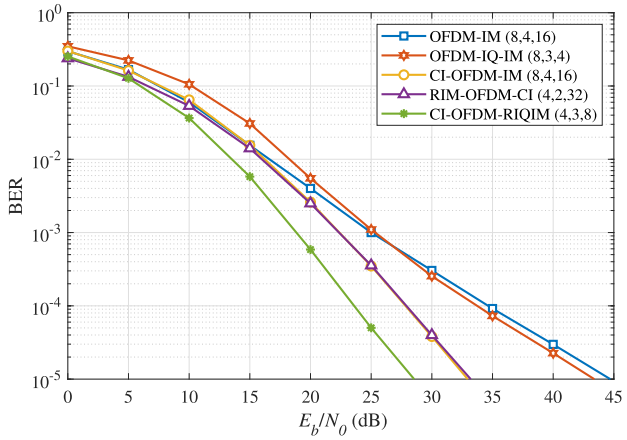

Fig. 9. Error performance comparison of CI-OFDM-RIQIM with benchmark schemes when at a spectral efficiency of 2.75 bps/Hz by utilizing LLR detectors.

in the CI-OFDM-IQIM by lower modulation order and the number of active subcarriers since the number of transmitted IM bits is quadrupled. Furthermore, it can be observed from Fig. 7 that CI-OFDM-RIQIM outperforms CI-OFDM-IQIM since more high-rank events are revealed as more subcarriers are activated in CI-OFDM-RIQIM when we consider the logic behind Fig. 3.

Fig. 8 shows an error performance comparison between the proposed and benchmark schemes, where the subblock size is four. It can be deduced from Fig. 8 that, CI-OFDM-IQIM remarkably outperforms CI-OFDM-RIQIM and reference schemes since the same data rate is provided with a lower modulation order by CI-OFDM-IQIM due to increased number of IM bits. Additionally, CI-OFDM-IQIM and CI-OFDM-RIQIM show better error performance compared to RIM-OFDM-CI while their spectral efficiency values are 14.3% higher.

In Fig. 9, CI-OFDM-RIQIM and the benchmark schemes are compared in terms of BER performance when spectral efficiency is 2.75 bps/Hz, $N_S = 8$, and LLR detectors are employed in all simulations. As seen from Fig. 9, approximately a 5 dB gain over RIM-OFDM-CI and CI-OFDM-IM is provided by CI-OFDM-RIQIM at a BER value of 10^{-5}.

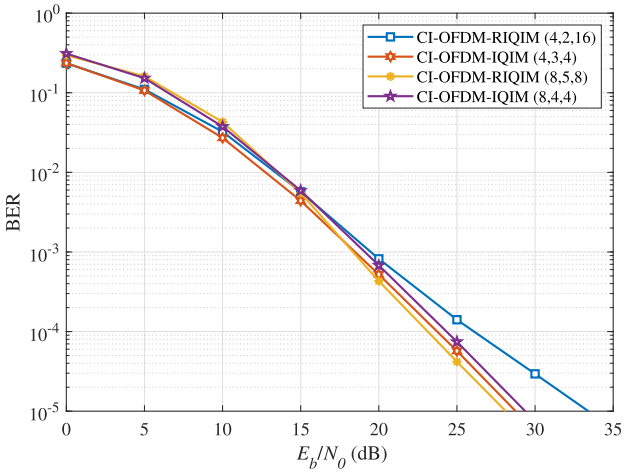

Fig. 10. Error performance comparison of CI-OFDM-RIQIM and CI-OFDM-IQIM for varying parameters at a spectral efficiency of 2.5 bps/Hz.

Furthermore, the same spectral efficiency is obtained by lower modulation order in CI-OFDM-RIQIM, resulting in enhanced error performance.

Error performances of CI-OFDM-RIQIM and CI-OFDM-IQIM for varying cluster sizes are investigated using LLR detectors in Fig. 10 where the spectral efficiency is 2.5 bps/Hz. As N_C increases, higher rank values are obtained more frequently and this explains the reason why CI-OFDM-RIQIM with higher subblock size outperforms other cases as seen from Fig. 10. On the other hand, CI-OFDM-IQIM demonstrates close error performance for the cases of $N_C = 4$ and $N_C = 8$.

While previous simulation results assume perfect CSI, the error performance of the proposed and existing schemes which also provide diversity order of two, is compared under the imperfect CSI conditions, in Fig. 11. For this, ML detection is performed by estimating $\hat{\mathbf{H}} = \text{diag}([\hat{h}_1, \cdots, \hat{h}_{N_S}]^{\text{T}})$ instead of the true $\mathbf{H}$ in (3) to decode the transmitted signal as in [32]. It is assumed that

$$\mathbf{H} = \hat{\mathbf{H}} + \mathbf{E}, \tag{16}$$

where $\mathbf{E} = \text{diag}([e_1, \cdots, e_{N_S}]^{\text{T}})$ denotes the matrix of channel estimation errors, whose elements follow $e_\alpha \sim \mathcal{CN}(0, \epsilon^2)$, $\alpha = 1, \cdots, N_S$, and ϵ^2 is the error variance where $\epsilon^2 \in [0, 1)$. Then, elements of the $\hat{\mathbf{H}}$ satisfies $\hat{h}_\alpha \sim \mathcal{CN}(0, 1 - \epsilon^2)$. Therefore, we obtain

$$h_\alpha = \hat{h}_\alpha + e_\alpha \tag{17}$$

for each sub-channel. Moreover, simulations in Fig. 11 are realized under the fixed CSI conditions with $\epsilon^2 = 0.05$ and $\epsilon^2 = 0.01$. As observed from Fig. 11, proposed schemes still outperform the reference schemes. For example, at a BER value of 10^{-5} and $\epsilon^2 = 0.01$, CI-OFDM-IQIM and CI-OFDM-RIQIM provide approximately 3 dB and 1 dB SNR gain over their closest rival, respectively.

A. Complexity Analysis

In Table II, a comparison of the decoding complexity per subcarrier of the proposed and benchmark schemes is given

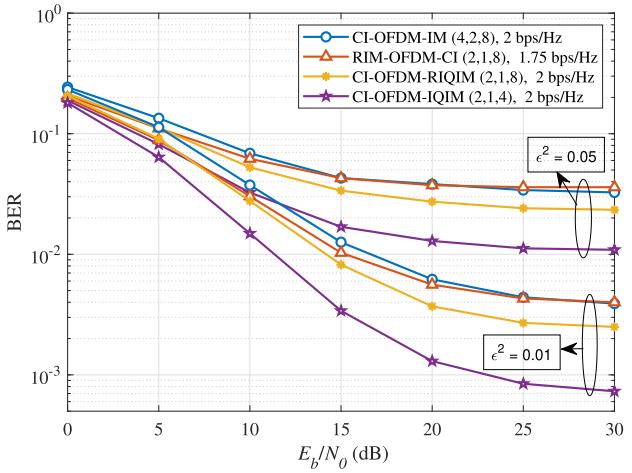

Fig. 11. Error performance comparison of CI-OFDM-RIQIM and CI-OFDM-IQIM with benchmark schemes under the imperfect CSI conditions for the parameters of $\epsilon^2 = 0.05$ and $\epsilon^2 = 0.01$.

TABLE II
DECODING COMPLEXITY COMPARISON PER SUBCARRIER

System	Detector	Complexity Order
OFDM	ML	$\mathcal{O}(M)$
OFDM-IM	Red. Comp. ML	$\mathcal{O}(M)$
CI-OFDM-IM	Red. Comp. ML	$\mathcal{O}(M^2)$
OFDM-IQ-IM	Red. Comp. ML	$\mathcal{O}(M)$
RIM-OFDM-CI	Suboptimal	$\mathcal{O}(M^2)$
CI-OFDM-RIQIM	Suboptimal	$\mathcal{O}(M^2)$
CI-OFDM-IQIM	Suboptimal	$\mathcal{O}(M)$

TABLE III
DECODING COMPLEXITY COMPARISON PER SUBBLOCK

System	Detector	CMs per subblock
OFDM-IM	Red. Comp. ML	$N_S M$
CI-OFDM-IM	Red. Comp. ML	$M(N_S M + K)$
OFDM-IQ-IM	Rec. Comp. ML	$2N_S M$
RIM-OFDM-CI	Suboptimal	$M(N_S M + 2K)$
CI-OFDM-RIQIM	ML	$M^{2K} 2^{2\left\lfloor \log_2 \binom{N_C}{K} \right\rfloor}$
CI-OFDM-RIQIM	Suboptimal	$M(N_S M + N_S + 2K)$
CI-OFDM-IQIM	ML	$M^{2K} 2^{4\left\lfloor \log_2 \binom{N_C}{K} \right\rfloor}$
CI-OFDM-IQIM	Suboptimal	$M(N_S + 2K)$

in terms of big $\mathcal{O}$ notation. As seen from Table II, the decoding complexity order of CI-OFDM-IQIM is equivalent to classical OFDM and OFDM-IM while providing better error performance and additional diversity gain. On the other hand, the decoding complexity of CI-OFDM-RIQIM increases exponentially with the modulation order. However, CI-OFDM-RIQIM shows superior error performance, and an interesting trade-off between the error performance and decoding complexity is presented.

To further investigate the complexity comparison between the proposed and reference schemes, we provide the number of complex multiplications (CMs) per subblock by considering the following parameters: modulation order (M), the number of active subcarriers (K), cluster length (N_C), and subblock length (N_S) in Table III. Moreover, by calculating the number of CMs per subblock, in Table IV, we provide a numerical example by considering the configurations in Fig. 7, Fig. 8, and Fig. 9. As seen from Table IV, the proposed low complexity LLR-based detector for CI-OFDM-IQIM reduces the decoding complexity significantly compared to the ML detector. Additionally, for the configuration of CI-OFDM-RIQIM in Fig. 9, the ML detector is not feasible, and the proposed detector reduces the complexity dramatically.

TABLE IV
A NUMERICAL EXAMPLE FOR COMPLEXITY COMPARISON

System	Detector	Fig. 7	Fig. 8	Fig. 9
OFDM-IM	Red. Comp. ML	16	16	128
CI-OFDM-IM	Red. Comp. ML	40	272	2112
OFDM-IQ-IM	Rec. Comp. ML	-	16	256
RIM-OFDM-CI	Suboptimal	144	272	8320
CI-OFDM-RIQIM	ML	1024	256	4194304
CI-OFDM-RIQIM	Suboptimal	60	304	624
CI-OFDM-IQIM	ML	1024	256	-
CI-OFDM-IQIM	Suboptimal	20	24	-

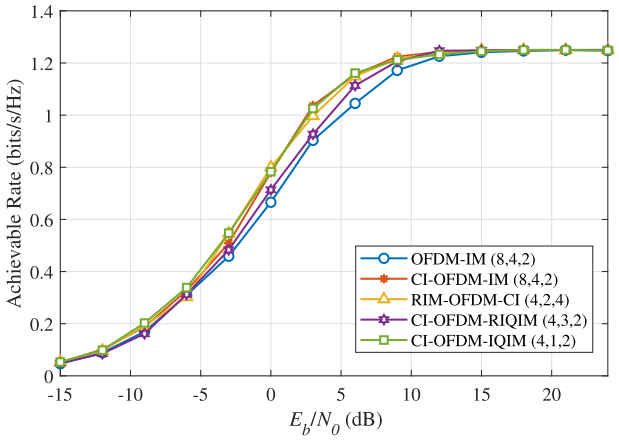

Fig. 12. Achievable rate comparison of CI-OFDM-RIQIM and CI-OFDM-IQIM with benchmark schemes at spectral efficiency of 1.25 bps/Hz.

B. Achievable Rate

In this subsection, we investigate the achievable rate performance of the proposed schemes and compare them to benchmark schemes. The achievable rate can be calculated numerically by exploiting the following expression presented in [41]:

$$R = \frac{1}{N_S}\left(b - \frac{1}{2^b}\sum_{\varsigma=1}^{2^b} \mathrm{E}_{\mathbf{h},\mathbf{n}}\left[\log_2 \sum_{\varrho=1}^{2^b} e^{\varpi(\varsigma,\varrho)}\right]\right), \qquad (18)$$

where $\varpi(\varsigma,\varrho) = \frac{-|\mathbf{H}(\mathbf{s}(\varsigma)-\mathbf{s}(\varrho))+\mathbf{n}|^2+|\mathbf{n}|^2}{N_0}$ and $\mathbf{H} = \mathrm{diag}(\mathbf{h})$.

In Fig. 12, the achievable rate performance of the proposed schemes is compared with benchmarks at spectral efficiency of 1.25 bps/Hz. As seen from Fig. 12, CI-OFDM-IQIM has approximately the same achievable rate performance as CI-OFDM-IM and RIM-OFDM-CI. Moreover, CI-OFDM-RIQIM outperforms OFDM-IM while providing close performance to CI-OFDM-IM and RIM-OFDM-CI.

V. CONCLUSION

In this paper, we have proposed a novel diversity achieving OFDM-IM based transmission scheme called CI-OFDM-RIQIM, which first divides all subblocks into two clusters and

transmits real and imaginary parts of the data symbols over the active subcarriers in these clusters. In addition, we have extended our contribution with another diversity-achieving scheme named CI-OFDM-IQIM by doubling information bits transmitted via IM. Moreover, LLR-based detectors have been designed for both schemes to reduce the overall system complexity. Finally, the error performances of the proposed schemes have been investigated by computer simulations. We conclude that CI-OFDM-RIQIM noticeably outperforms the reference schemes since data bits conveyed by IM are increased. Furthermore, CI-OFDM-IQIM shows superior error performance for higher spectral efficiency values since doubled information bits transmitted by IM enable the system to obtain the same spectral efficiency by lower modulation orders. In addition, designed LLR detectors noticeably reduce the detection complexity while still providing superior error performances. Eventually, their diversity gain, remarkable error performance, and higher spectral efficiency make the proposed schemes appropriate candidates for next-generation communication services. The generalization of the proposed schemes for more than 2 clusters is left as a future study item.

REFERENCES

[1] E. Başar, U. Aygölü, E. Panayırcı, and H. V. Poor, "Orthogonal frequency division multiplexing with index modulation," *IEEE Trans. Signal Process.*, vol. 61, no. 22, pp. 5536–5549, Nov. 2013.

[2] R. Fan, Y. J. Yu, and Y. L. Guan, "Orthogonal frequency division multiplexing with generalized index modulation," in *Proc. IEEE Global Commun. Conf.*, Dec. 2014, pp. 3880–3885.

[3] B. Zheng, F. Chen, M. Wen, F. Ji, H. Yu, and Y. Liu, "Low-complexity ML detector and performance analysis for OFDM with in-phase/quadrature index modulation," *IEEE Commun. Lett.*, vol. 19, no. 11, pp. 1893–1896, Nov. 2015.

[4] M. Wen, B. Ye, E. Basar, Q. Li, and F. Ji, "Enhanced orthogonal frequency division multiplexing with index modulation," *IEEE Trans. Wireless Commun.*, vol. 16, no. 7, pp. 4786–4801, Jul. 2017.

[5] A. M. Jaradat, J. M. Hamamreh, and H. Arslan, "OFDM with subcarrier number modulation," *IEEE Wireless Commun. Lett.*, vol. 7, no. 6, pp. 914–917, Dec. 2018.

[6] J. Li, S. Dang, M. Wen, X. Jiang, Y. Peng, and H. Hai, "Layered orthogonal frequency division multiplexing with index modulation," *IEEE Syst. J.*, vol. 13, no. 4, pp. 3793–3802, Dec. 2019.

[7] Y. Xiao, S. Wang, L. Dan, X. Lei, P. Yang, and W. Xiang, "OFDM with interleaved subcarrier-index modulation," *IEEE Commun. Lett.*, vol. 18, no. 8, pp. 1447–1450, Aug. 2014.

[8] L. Xiao, G. Liu, P. Xiao, and T. Jiang, "Error probability analysis for rectangular differential OFDM with index modulation over dispersive channels," *IEEE Wireless Commun. Lett.*, vol. 10, no. 12, pp. 2795–2799, Dec. 2021.

[9] A. M. Jaradat, J. M. Hamamreh, and H. Arslan, "OFDM with hybrid number and index modulation," *IEEE Access*, vol. 8, pp. 55042–55053, 2020.

[10] E. Arslan, A. T. Dogukan, and E. Basar, "Sparse-encoded codebook index modulation," *IEEE Trans. Veh. Technol.*, vol. 69, no. 8, pp. 9126–9130, Aug. 2020.

[11] E. Basar, "On multiple-input multiple-output OFDM with index modulation for next generation wireless networks," *IEEE Trans. Signal Process.*, vol. 64, no. 15, pp. 3868–3878, Aug. 2016.

[12] S. Lu, I. A. Hemadeh, M. El-Hajjar, and L. Hanzo, "Compressed-sensing-aided space-time frequency index modulation," *IEEE Trans. Veh. Technol.*, vol. 67, no. 7, pp. 6259–6271, Jul. 2018.

[13] R. Chen and J. Zheng, "Index-modulated MIMO-OFDM: Joint space-frequency signal design and linear precoding in rapidly time-varying channels," *IEEE Trans. Wireless Commun.*, vol. 17, no. 10, pp. 7067–7079, Oct. 2018.

[14] L. Wang, "Generalized quadrature space-frequency index modulation for MIMO-OFDM systems," *IEEE Trans. Commun.*, vol. 69, no. 9, pp. 6375–6389, Sep. 2021.

[15] A. Tusha, S. Dogan, and H. Arslan, "A hybrid downlink NOMA with OFDM and OFDM-IM for beyond 5G wireless networks," *IEEE Signal Process. Lett.*, vol. 27, pp. 491–495, 2020.

[16] X. Chen, M. Wen, and S. Dang, "On the performance of cooperative OFDM-NOMA system with index modulation," *IEEE Wireless Commun. Lett.*, vol. 9, no. 9, pp. 1346–1350, Sep. 2020.

[17] S. Dogan, A. Tusha, and H. Arslan, "NOMA with index modulation for uplink URLLC through grant-free access," *IEEE J. Sel. Topics Signal Process.*, vol. 13, no. 6, pp. 1249–1257, Oct. 2019.

[18] E. Arslan, A. T. Dogukan, and E. Basar, "Index modulation-based flexible non-orthogonal multiple access," *IEEE Wireless Commun. Lett.*, vol. 9, no. 11, pp. 1942–1946, Nov. 2020.

[19] M. M. Sahin and H. Arslan, "Waveform-domain NOMA: The future of multiple access," in *Proc. IEEE Int. Conf. Commun. Workshops*, Jun. 2020, pp. 1–6.

[20] M. M. Şahin, I. E. Gurol, E. Arslan, E. Basar, and H. Arslan, "OFDM-IM for joint communication and radar-sensing: A promising waveform for dual functionality," *Frontiers Commun. Netw.*, vol. 2, p. 34, Aug. 2021.

[21] A. W. Azim, Y. Le Guennec, M. Chafii, and L. Ros, "Enhanced optical-OFDM with index and dual-mode modulation for optical wireless systems," *IEEE Access*, vol. 8, pp. 128646–128664, 2020.

[22] E. Basar and E. Panayirci, "Optical OFDM with index modulation for visible light communications," in *Proc. 4th Int. Workshop Opt. Wireless Commun. (IWOW)*, Sep. 2015, pp. 11–15.

[23] T. Mao, Z. Wang, Q. Wang, S. Chen, and L. Hanzo, "Dual-mode index modulation aided OFDM," *IEEE Access*, vol. 5, pp. 50–60, 2017.

[24] T. Mao, Q. Wang, and Z. Wang, "Generalized dual-mode index modulation aided OFDM," *IEEE Commun. Lett.*, vol. 21, no. 4, pp. 761–764, Apr. 2017.

[25] M. Wen, E. Basar, Q. Li, B. Zheng, and M. Zhang, "Multiple-mode orthogonal frequency division multiplexing with index modulation," *IEEE Trans. Commun.*, vol. 65, no. 9, pp. 3892–3906, Sep. 2017.

[26] M. Wen, Q. Li, E. Basar, and W. Zhang, "Generalized multiple-mode OFDM with index modulation," *IEEE Trans. Wireless Commun.*, vol. 17, no. 10, pp. 6531–6543, Oct. 2018.

[27] F. Yarkin and J. P. Coon, "Q-ary multi-mode OFDM with index modulation," *IEEE Wireless Commun. Lett.*, vol. 9, no. 7, pp. 1110–1114, Jul. 2020.

[28] F. Yarkin and J. P. Coon, "Modulation based on a simple MDS code: Achieving better error performance than index modulation and related schemes," *IEEE Trans. Commun.*, vol. 70, no. 1, pp. 118–131, Jan. 2022.

[29] A. T. Dogukan and E. Basar, "Super-mode OFDM with index modulation," *IEEE Trans. Wireless Commun.*, vol. 19, no. 11, pp. 7353–7362, Nov. 2020.

[30] F. Yarkin and J. P. Coon, "Set partition modulation," *IEEE Trans. Wireless Commun.*, vol. 19, no. 11, pp. 7557–7570, Nov. 2020.

[31] J. Zheng and R. Chen, "Achieving transmit diversity in OFDM-IM by utilizing multiple signal constellations," *IEEE Access*, vol. 5, pp. 8978–8988, 2017.

[32] T. V. Luong, Y. Ko, and J. Choi, "Repeated MCIK-OFDM with enhanced transmit diversity under CSI uncertainty," *IEEE Trans. Wireless Commun.*, vol. 17, no. 6, pp. 4079–4088, Jun. 2018.

[33] J. Choi, "Coded OFDM-IM with transmit diversity," *IEEE Trans. Commun.*, vol. 65, no. 7, pp. 3164–3171, Jul. 2017.

[34] E. Basar, "OFDM with index modulation using coordinate interleaving," *IEEE Wireless Commun. Lett.*, vol. 4, no. 4, pp. 381–384, Aug. 2015.

[35] A. T. Dogukan and E. Basar, "Orthogonal frequency division multiplexing with power distribution index modulation," *Electron. Lett.*, vol. 56, no. 21, pp. 1156–1159, Oct. 2020.

[36] A. T. Dogukan, O. F. Tugtekin, and E. Basar, "Coordinate interleaved OFDM with power distribution index modulation," *IEEE Commun. Lett.*, vol. 26, no. 8, pp. 1908–1912, Aug. 2022.

[37] H. L. T. Thanh, V. Ngo, M. Le, and X. N. Tran, "Repeated index modulation with coordinate interleaved OFDM," in *Proc. 5th NAFOSTED Conf. Inf. Comput. Sci. (NICS)*, Nov. 2018, pp. 114–118.

[38] T. T. H. Le, X. N. Tran, V. Ngo, and M. Le, "Repeated index modulation-OFDM with coordinate interleaving: Performance optimization and low-complexity detectors," *IEEE Syst. J.*, vol. 15, no. 3, pp. 3673–3681, Sep. 2021.

[39] T. Mao, Q. Wang, Z. Wang, and S. Chen, "Novel index modulation techniques: A survey," *IEEE Commun. Surveys Tuts.*, vol. 21, no. 1, pp. 315–348, 1st Quart., 2019.

[40] M. Z. A. Khan and B. S. Rajan, "Single-symbol maximum likelihood decodable linear STBCs," *IEEE Trans. Inf. Theory*, vol. 52, no. 5, pp. 2062–2091, May 2006.

[41] N. Ishikawa, S. Sugiura, and L. Hanzo, "Subcarrier-index modulation aided OFDM—Will it work?" *IEEE Access*, vol. 4, pp. 2580–2593, 2016.